Supplementary Information (SI) for Energy & Environmental Science.
This journal is © The Royal Society of Chemistry 2026

Supplementary Information for

3D Imaging-Informed Electrode Engineering for Water Splitting

Authors: Shuhao Wang[1], Omid Tavakkoli[3], Mohamed Regaieg[4], Christoph Sachs[5], David Ayme-Perrot[5], Hubert Girault[6], Quentin Meyer[1], Ying Da Wang[2], Ryan Armstrong[3], Chuan Zhao[1], Peyman Mostaghimi[3]*

Affiliations:

[1]School of Chemistry, The University of New South Wales, Sydney, Australia.
[2]School of Minerals and Energy Resources Engineering, The University of New South Wales, Sydney, Australia.
[3]School of Civil and Environmental Engineering, The University of New South Wales, Sydney, Australia.
[4]TotalEnergies, OneTech, Pau, France.
[5]TotalEnergies SE, OneTech, Tour Coupole - 2 place Jean Millier - 92078 Paris La Défense cedex, France
[6]Institute of Chemical Sciences and Engineering, École Polytechnique Fédéralede Lausanne, Lausanne, Switzerland

*Corresponding author. Email: peyman@unsw.edu.au

The PDF file includes:

Supplementary Notes 1 to 2
Supplementary Figures 1 to 22
Supplementary Tables 1
Supplementary References

Supplementary Notes 1

Fast Fourier transform (FFT) simulation

The variations in dynamic resistance were analyzed in the frequency domain using a discrete Fourier transform (FFT) function implemented in MATLAB®. Characteristic amplitude peaks embedded in the resistance signal were identified and subsequently smoothed by applying a 4th-order Savitzky–Golay filter through the sgolayfilt function in MATLAB.[1]

```
%% Step 0. Read data
data = readmatrix('C:\Users\wang2\Desktop\eisoer.txt');
t = data(:,1);              % Time (s)
Z = data(:,4);               % Z (Ohm)

%% Step 1. Sampling parameters
dt = t(2)-t(1);             % Time step
Fs = 1/dt;                    % Sampling frequency
T = dt;                        % Sampling period
L = length(Z);              % Signal length

%% Step 2. FFT (make sure single-sided spectrum and frequency vector have equal length)
Y = fft(Z);
P2 = abs(Y/L);

if mod(L,2)==0
    % Even number of points
    P1 = P2(1:L/2+1);
else
    % Odd number of points
    P1 = P2(1:(L+1)/2);
end

if numel(P1) > 2
    P1(2:end-1) = 2*P1(2:end-1);    % Single-sided spectrum correction
end

% Frequency vector, same length as P1
f = Fs*(0:numel(P1)-1)/L;

%% Step 3. Smoothing (Savitzky-Golay, robust windowing)
order = 3;
framelen = 51;
% Apply smoothing only on P1(2:end); window must be odd and not exceed data length
effLen = max(numel(P1(2:end)), 1);
```

```
framelen = min(framelen, 2*floor((effLen-1)/2)+1);
if framelen < order+2
    framelen = order+2;
    if mod(framelen,2)==0, framelen = framelen+1; end
    framelen = min(framelen, effLen - (1-mod(effLen,2)));
end
if mod(framelen,2)==0, framelen = framelen-1; end

P1_smooth = P1;
if effLen >= framelen && framelen >= order+2 && numel(P1)>2
    P1_smooth(2:end) = sgolayfilt(P1(2:end), order, framelen);
end

%% Step 4. Envelope (same length as P1)
[e_upper, ~] = envelope(P1, 10, 'peak');

%% Step 4.1 Safety alignment (prevent mismatch length errors)
npts = min([numel(f), numel(P1), numel(P1_smooth), numel(e_upper)]);
f           = f(1:npts);
P1          = P1(1:npts);
P1_smooth   = P1_smooth(1:npts);
e_upper     = e_upper(1:npts);

%% Step 4.5    Reduce envelope to single-number metrics
% Frequency band (same as in the plot)
fmin = 0.0;
fmax = 0.2;

idx = (f >= fmin) & (f <= fmax);

% If no points in the band, fall back to the full band
if ~any(idx)
    idx = true(size(f));
    fmin_eff = min(f);
    fmax_eff = max(f);
else
    fmin_eff = fmin;
    fmax_eff = fmax;
end

f_band = f(idx);
e_band = e_upper(idx);
```

```
% Peak envelope and its frequency
[peak_env, kpeak] = max(e_band);
if ~isempty(kpeak)
    f_peak_env = f_band(kpeak);
else
    f_peak_env = NaN;
end

% Mean and RMS of envelope in the band
mean_env = mean(e_band);
rms_env    = sqrt(mean(e_band.^2));

% Area under the envelope curve and normalized value
auc_env    = trapz(f_band, e_band);
bw           = max(fmax_eff - fmin_eff, eps);
auc_norm = auc_env / bw;

%% Step 5. Plotting
figure; hold on;
plot(f, P1, 'Color',[0.7 0.7 0.7], 'LineWidth',0.8, 'DisplayName','Raw Spectrum');
plot(f, P1_smooth, 'Color',[228/255 26/255 28/255], 'LineWidth',1.5,
'DisplayName','Smoothed Fit');
plot(f, e_upper, 'Color',[0.2 0.2 0.2], 'LineWidth',1, 'DisplayName','Envelope');

% Mark envelope peak
if ~isnan(f_peak_env) && ~isnan(peak_env)
    plot(f_peak_env, peak_env, 'ko', 'MarkerFaceColor','k', 'DisplayName','Envelope Peak');
end

xlabel('f (Hz)');
ylabel('Amplitude (a.u.)');
title('');
legend('show','Location','northeast');
xlim([0 0.2]);
ylim([-0.5e-3 3e-3]);
set(gca,'FontSize',12);
grid on; box on;

%% Step 6. Save spectrum and envelope data to TXT
f_col = f(:);
P1_col = P1(:);
P1_smooth_col = P1_smooth(:);
e_upper_col = e_upper(:);
```

```
output_data = [f_col, P1_col, P1_smooth_col, e_upper_col];
output_filename = 'C:\Users\wang2\Desktop\fft_result.txt';
% Write header
fid = fopen(output_filename,'w');
fprintf(fid, 'Frequency(Hz)\tRawSpectrum\tSmoothFit\tEnvelope\n');
fclose(fid);

% Write main data
dlmwrite(output_filename, output_data, '-append', 'delimiter', '\t', 'precision', '%.6e');

%% Step 6.1 Append single-number metrics at the end
fid = fopen(output_filename,'a');
fprintf(fid, '\n# Envelope single-number metrics in [%.6g, %.6g] Hz (effective band)\n',
fmin_eff, fmax_eff);
fprintf(fid, '# peak_env\tf_peak_env(Hz)\tmean_env\trms_env\tauc_env\tauc_norm\n');
fprintf(fid, '%.6e\t%.6e\t%.6e\t%.6e\t%.6e\t%.6e\n', ...
            peak_env, f_peak_env, mean_env, rms_env, auc_env, auc_norm);
fclose(fid);
```

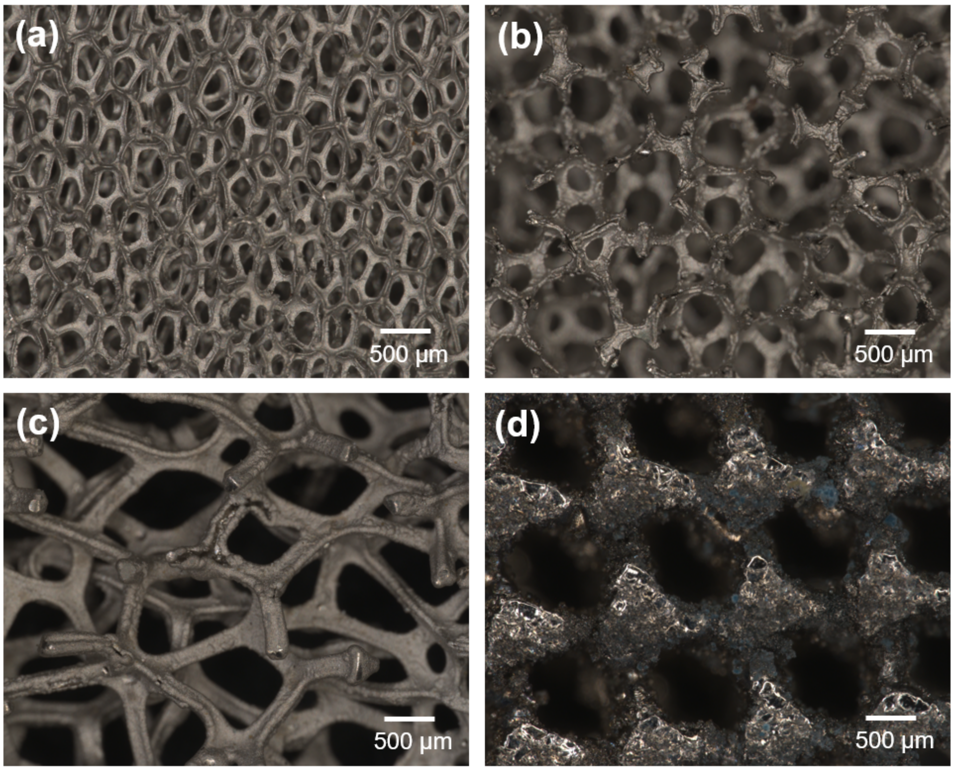

Supplementary Figure 1. Optical microscopy of highly-ordered square electrode commercial nickel foams with varying pore densities (20–130 ppi) and 3 mm thickness; (a) 130 ppi, (b) 60 ppi, (c) 20 ppi, and (d) square electrode.

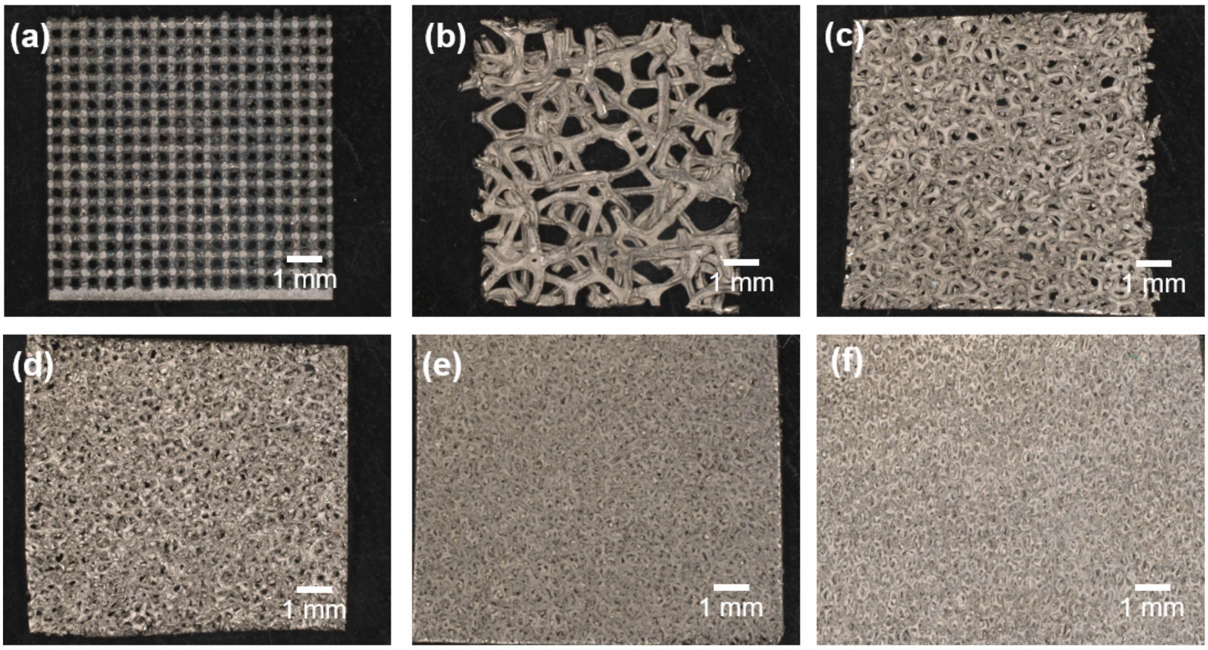

Supplementary Figure 2. Optical microscopy of highly-ordered square electrode and commercial Ni foams with varying pore densities (20–130 ppi) and 0.5 mm thickness, pristine ones compressed under a pressure of 20 kPa into thin sheets; (a) square electrode, (b) 20 ppi, (c) 40 ppi, (d) 60 ppi, (e) 100 ppi, and (f) 130 ppi.

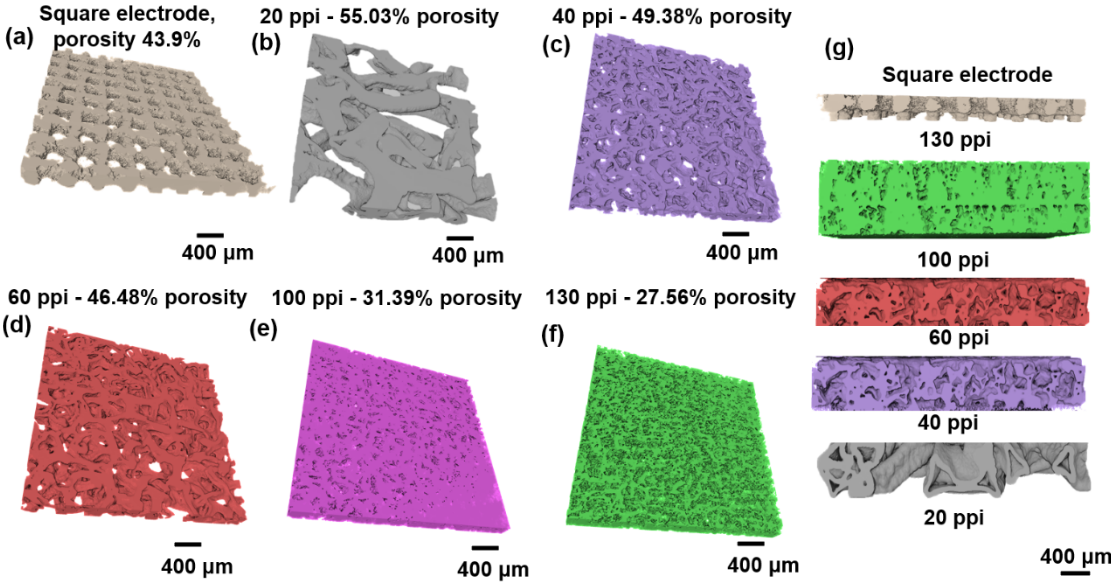

Supplementary Figure 3. (a) 3D X-ray micro-tomography reconstructions of highly-ordered square electrode (b–f) 3D X-ray micro-tomography reconstructions of nickel foams with varying pore densities (20–130 ppi), showing differences in porosity and internal architecture. (g) Side-view cross-sections of the compressed metal electrodes (500 µm thick).

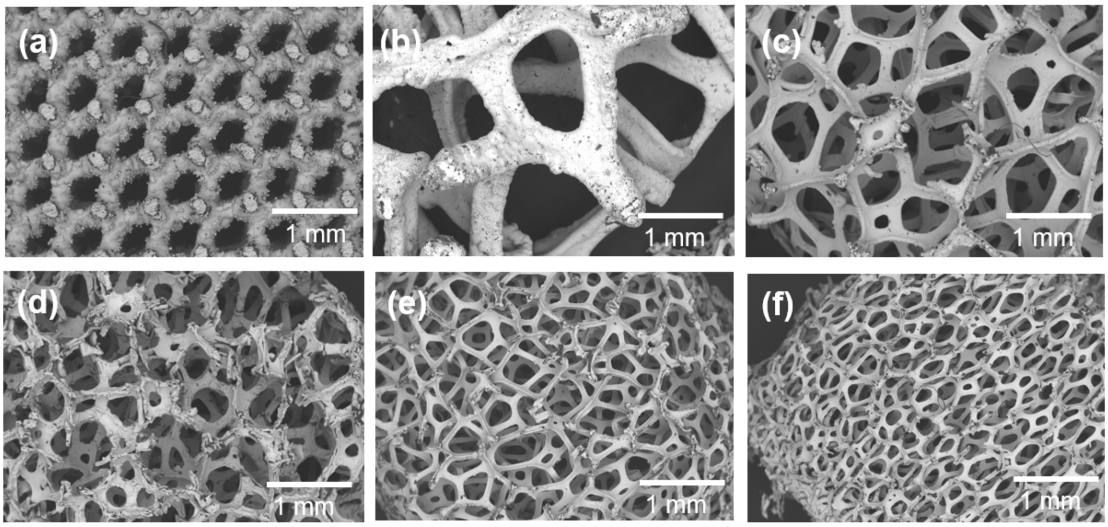

Supplementary Figure 4. (a) SEM images of highly-ordered square electrode (a) and (b-f) Ni foams with varying pore densities (20–130 ppi); (b) 20 ppi, (c) 40 ppi, (d) 60 ppi, (e) 100 ppi, and (f) 130 ppi.

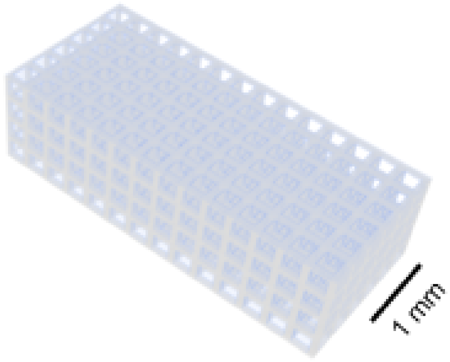

Supplementary Figure 5. Synthetic highly-ordered square electrode.

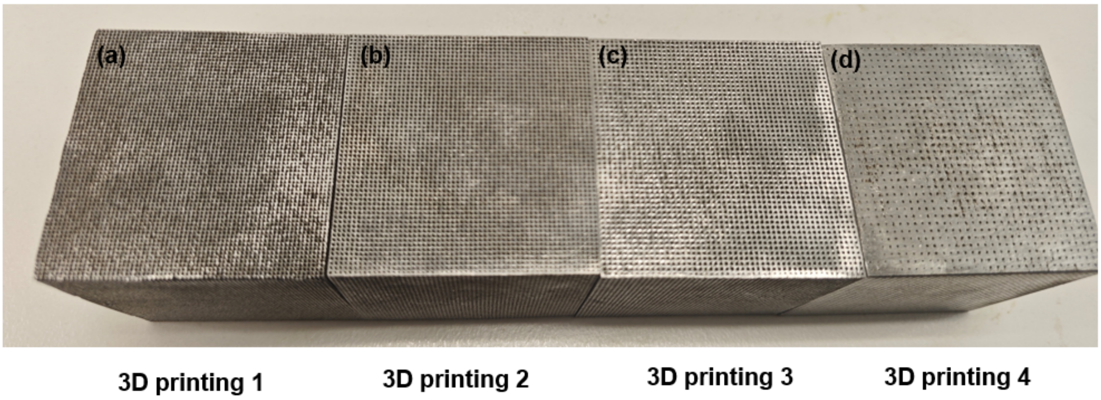

Supplementary Figure 6. Digital photos of four types of highly-ordered square electrodes with beam thicknesses (a) 0.2 mm, (b) 0.3 mm; (c) 0.4 mm; (d) 0.8 mm for a 0.4 mm pore size.

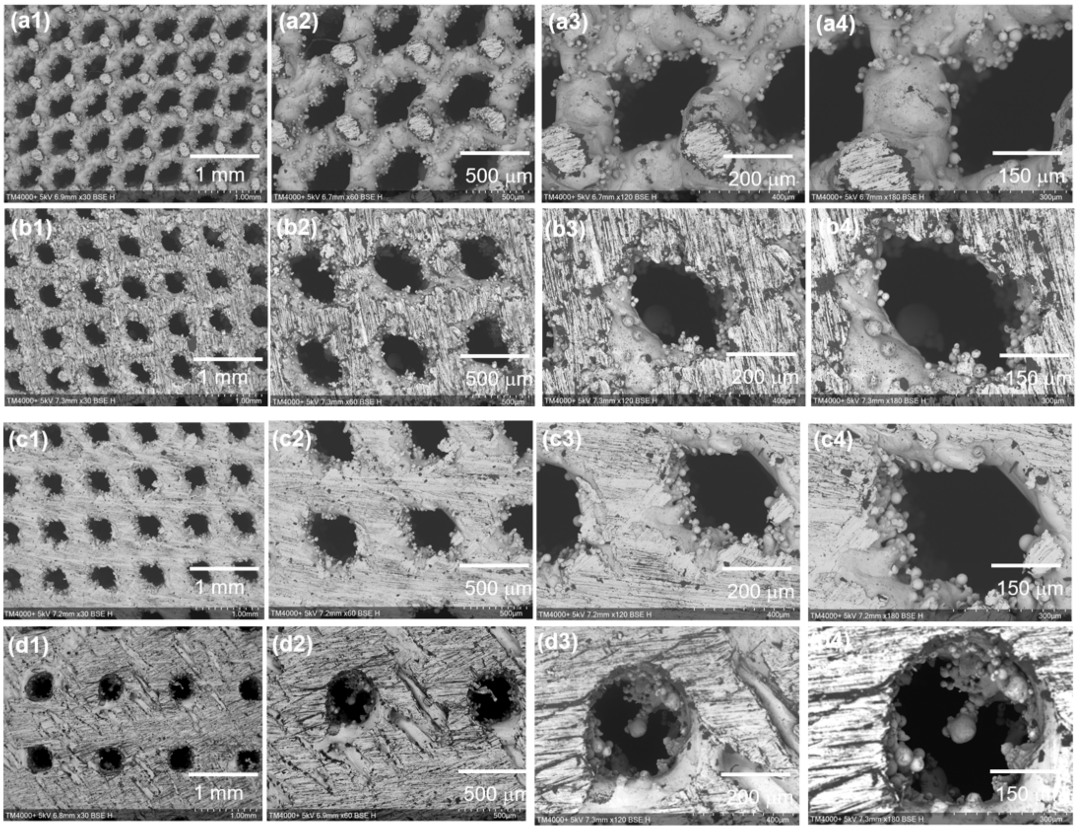

Supplementary Figure 7. SEM images of four types of highly-ordered square made by 3D-printing with varying beam thicknesses and constant void size (0.4 mm): (a) beam thickness 0.2 mm; (b) beam thickness 0.3 mm; (c) beam thickness 0.4 mm; (d) beam thickness 0.8 mm.

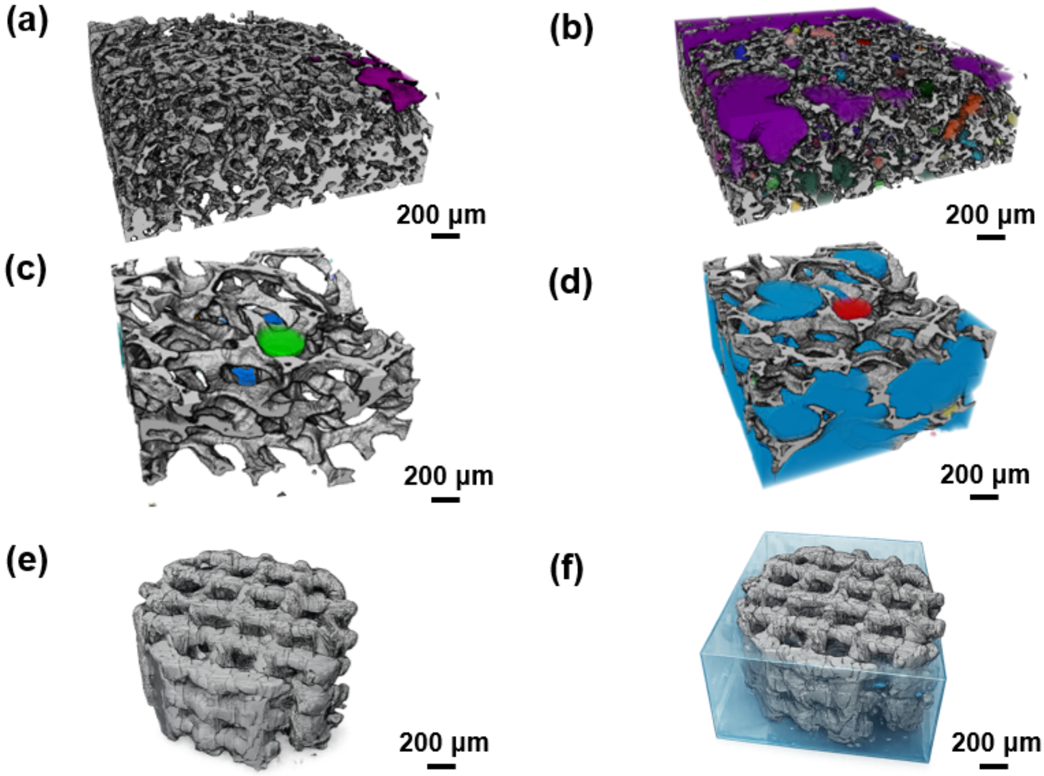

Supplementary Figure 8. Conventional laboratory-based micro-CT imaging before and after electrolysis, illustrating gas entrapment within porous electrodes: (a) 130 ppi nickel foam before reaction; (b) 130 ppi nickel foam after reaction; (c) 60 ppi nickel foam before reaction; (d) 60 ppi nickel foam after reaction; (e) highly-ordered square electrode before reaction; (f) highly-ordered square electrode after reaction. The gray regions represent the metallic framework of the porous electrode. Colored regions correspond to trapped gas bubbles, where the same color denotes a single continuous gas domain.

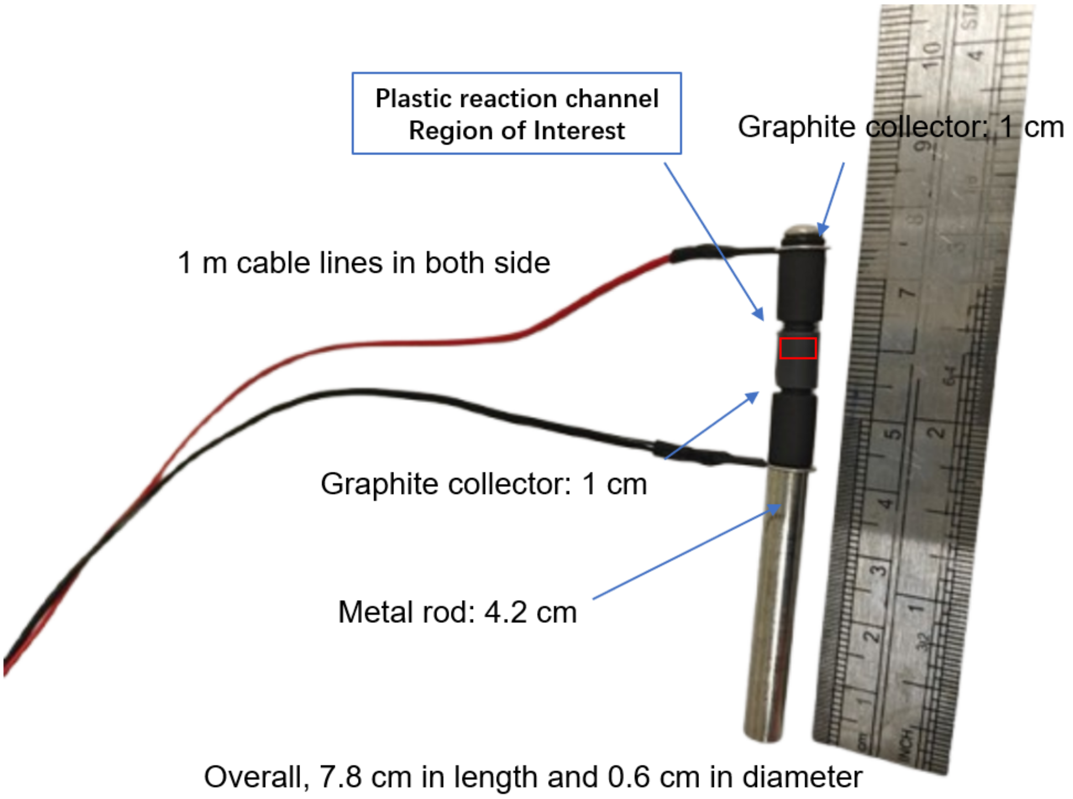

Supplementary Figure 9. Photograph and dimensional breakdown of the *operando* cell design used for X-ray micro-CT imaging.

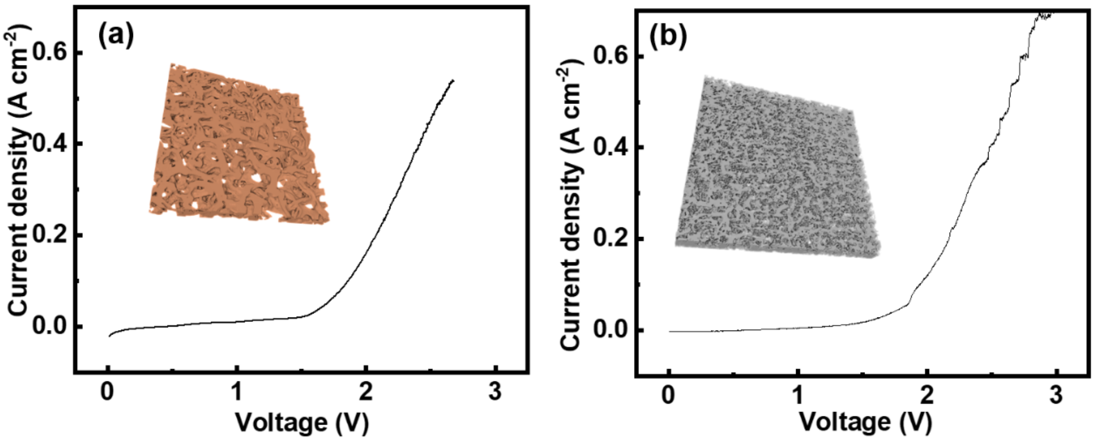

Supplementary Figure 10. Linear sweep voltammetry (LSV) curves of (a) 60 ppi and (b) 130 ppi nickel foam electrodes measured in 1 M KOH containing 30 wt% KI in the *operando* cell with 95% *iR* compensation.

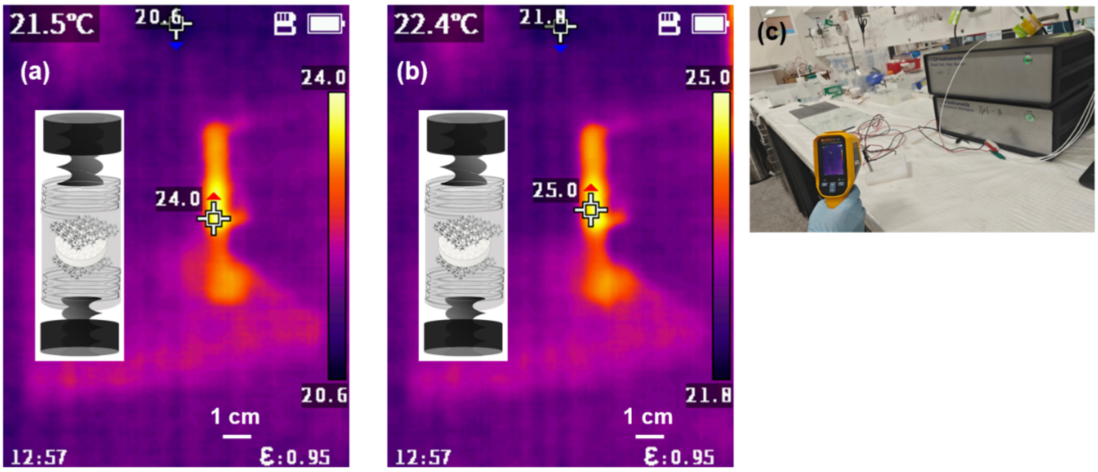

Supplementary Figure 11. Infrared thermal images of the *operando* electrochemical cell recorded before (a) and after reaction (b) using a FLUKE VT06 thermal imaging camera, and (c) a photograph of the thermal imaging setup during electrolysis.

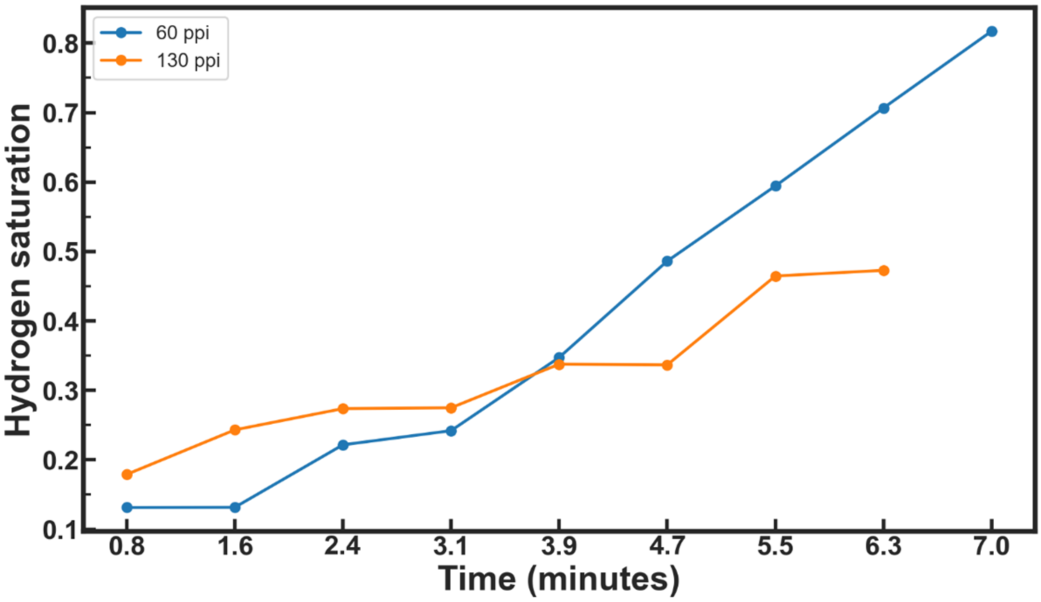

Supplementary Figure 12. Hydrogen saturation rate based on *operando* micro-CT results on 60 and 130 ppi nickel foams.

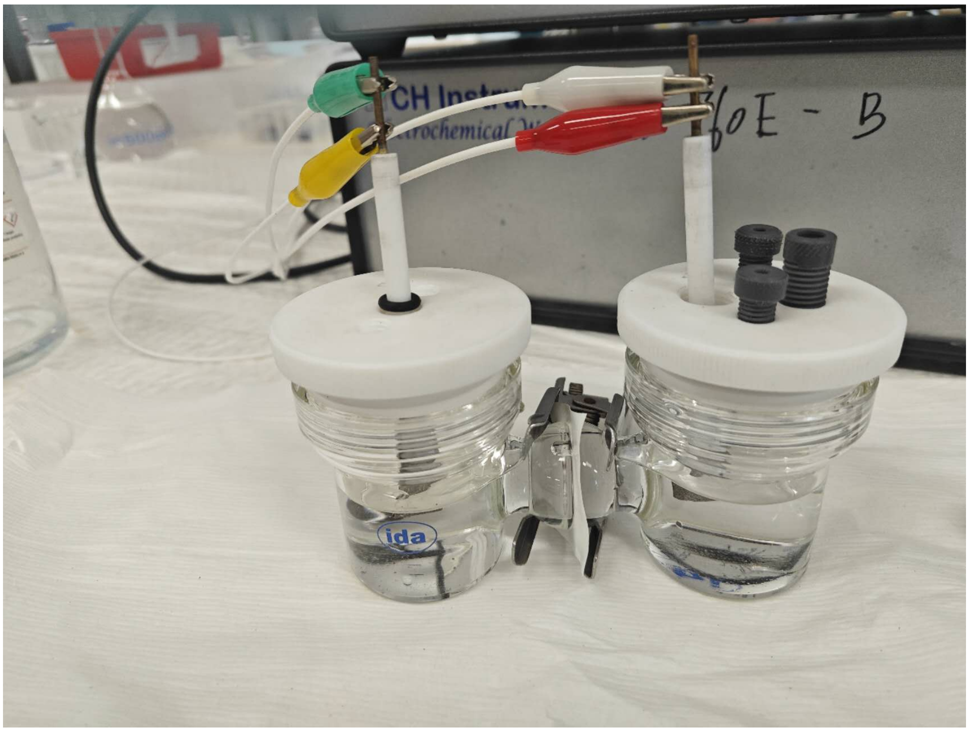

Supplementary Figure 13. Photograph of the two-compartment H-cell setup with 30 wt% KOH and Zirfon UTP 220 membrane.

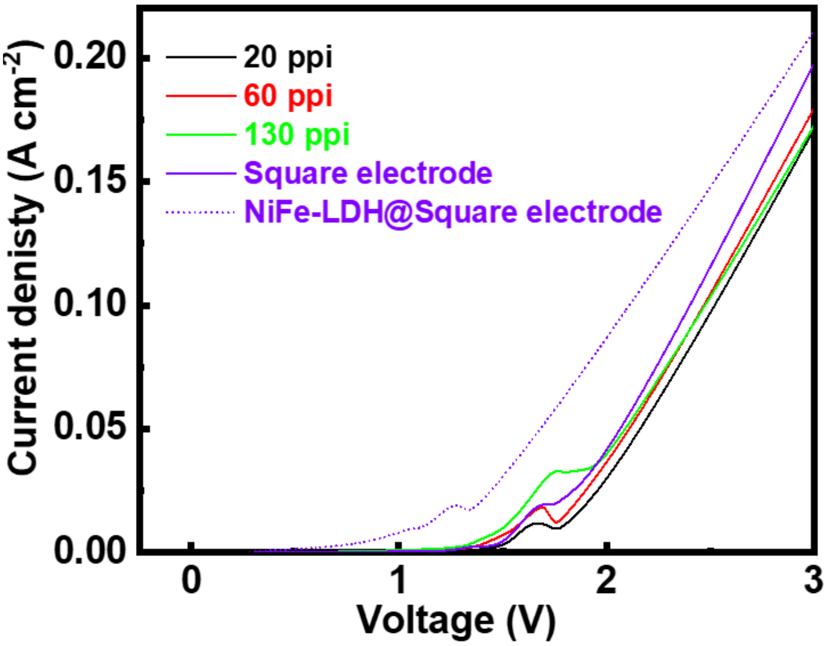

Supplementary Figure 14. Linear sweep voltammetry (LSV) curves of nickel foam electrodes with varying pore densities, highly ordered square electrode, highly-order square electrode with NiFe-LDH catalysts under H-cell conditions for two-electrode reaction with 30 wt% KOH and ZIRFON membrane.

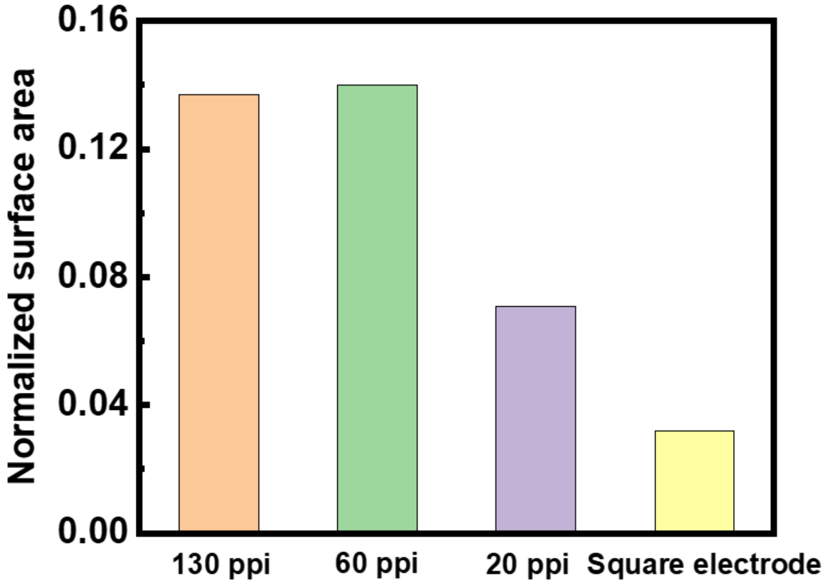

Supplementary Figure 15. Normalized solid–liquid interfacial surface area of Ni foams with varying pore densities, calculated from LBM simulations based on micro-CT reconstructed geometries.

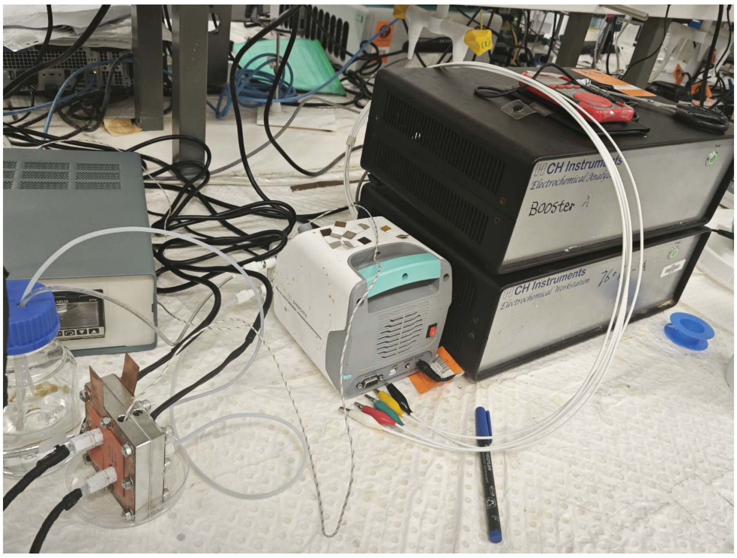

Supplementary Figure 16. Photograph of the full-cell electrolyser setup.

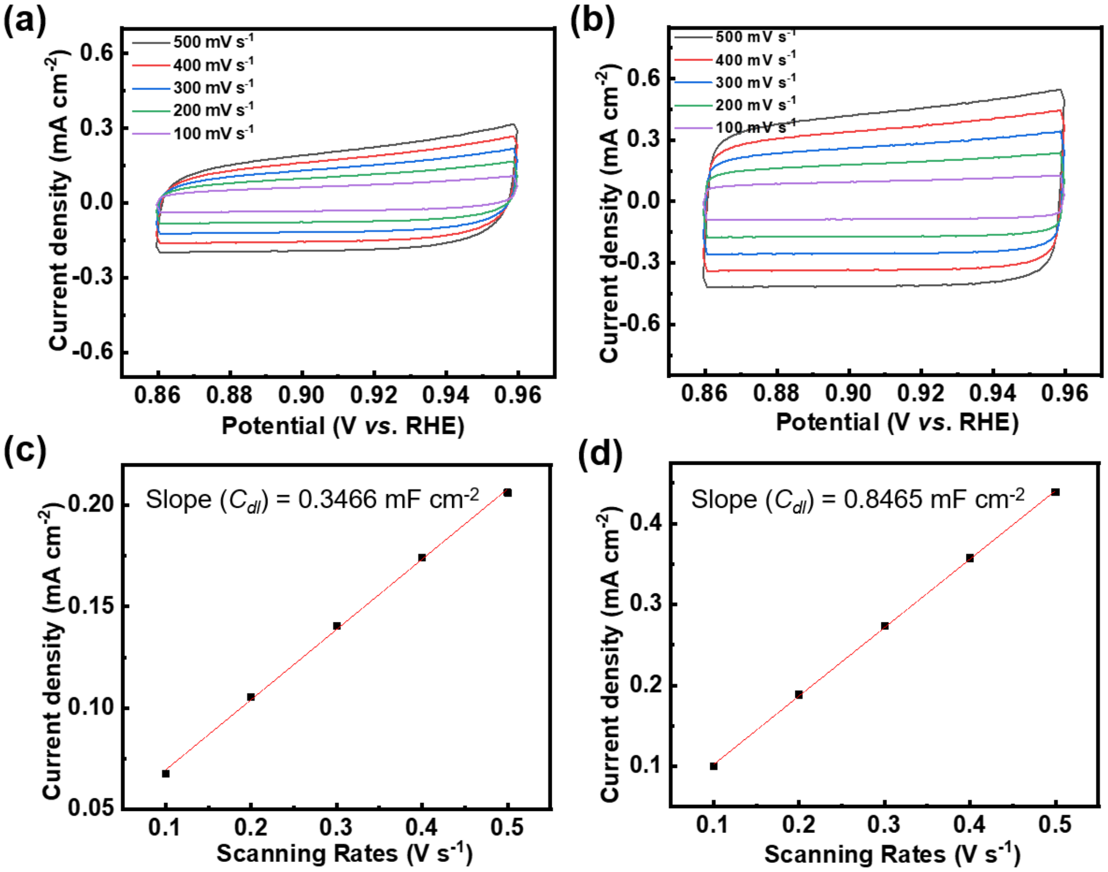

Supplementary Figure 17. Cyclic voltammetry curves at various scan rates during non-Faradaic conditions (0.86-0.96 V *vs.* RHE) on (a) highly-ordered square-grid electrode and (b) 60 ppi nickel foam; Relevant fitting for electrochemical surface areas by cyclic voltammetry results on (c) highly-ordered square-grid electrode and (d) 60 ppi nickel foam.

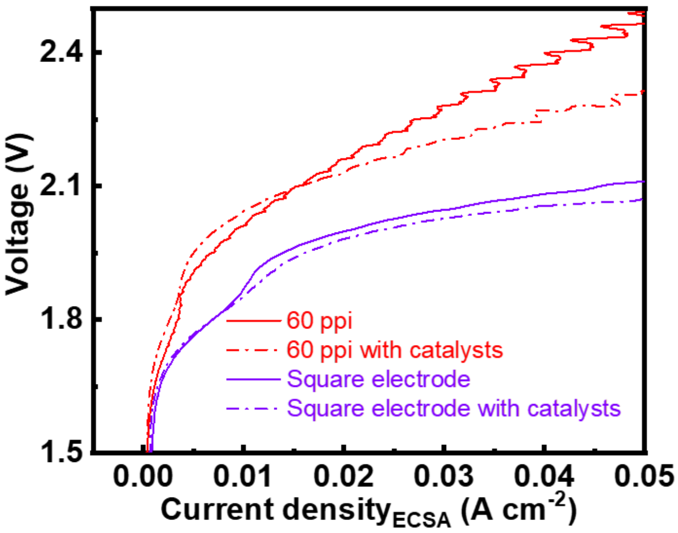

Supplementary Figure 18. ECSA normalized polarization curves of 60 ppi and highly-ordered square-grid electrode in MEA. The ECSA was determined under non-Faradaic conditions (0.86-0.96 V *vs.* RHE) in the absence of gas bubbles and uniformly applied for normalization across all current densities.

Supplementary Notes 2

The ECSA values used to normalize the polarization curves in Supplementary Figure 18 were determined from double-layer capacitance measurements conducted under non-Faradaic conditions (0.86–0.96 V vs. RHE), where no significant gas evolution occurs (Supplementary Fig. 17). The extracted ECSA for each electrode was then uniformly applied across the entire current density range.

It should be noted that this measurement reflects the electrochemically accessible surface area under bubble-free conditions. Under high-current-density operation (e.g., 2 $A \cdot cm^{-2}$), substantial bubble generation may cover the active sites, particularly in nickel foams. Consequently, the effective "operating ECSA" during practical electrolysis can be lower than the static ECSA value. In contrast, the highly ordered square architecture, owing to its enhanced bubble detachment and reduced gas trapping, is expected to retain a larger fraction of electrochemically accessible surface under load.

Therefore, while the ECSA-normalized curves represent intrinsic surface-area-normalized activity under static conditions, differences in bubble coverage at high current densities may further amplify the effective performance gap between the ordered lattice and conventional foams. This highlights the limitation of conventional ECSA measurements in fully capturing dynamic surface accessibility in gas-evolving systems and motivates future approaches aimed at quantifying the operating ECSA under realistic reaction conditions.

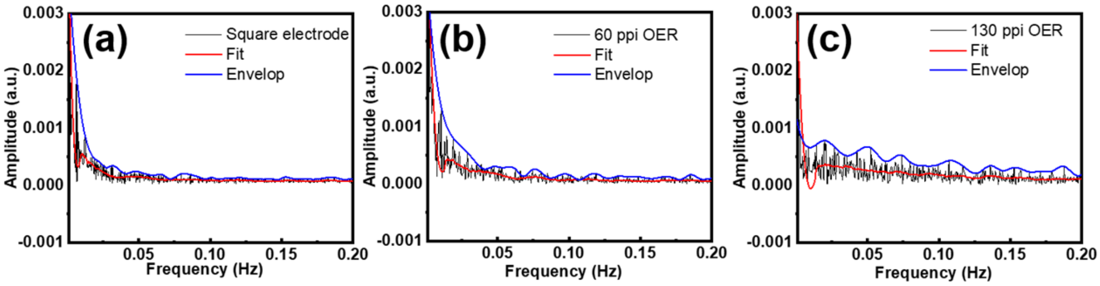

Supplementary Figure 19. FFT analysis of the impedance fluctuations corresponding to (a) highly ordered square electrode, (b) 60 ppi, and (c) 130 ppi nickel foam.

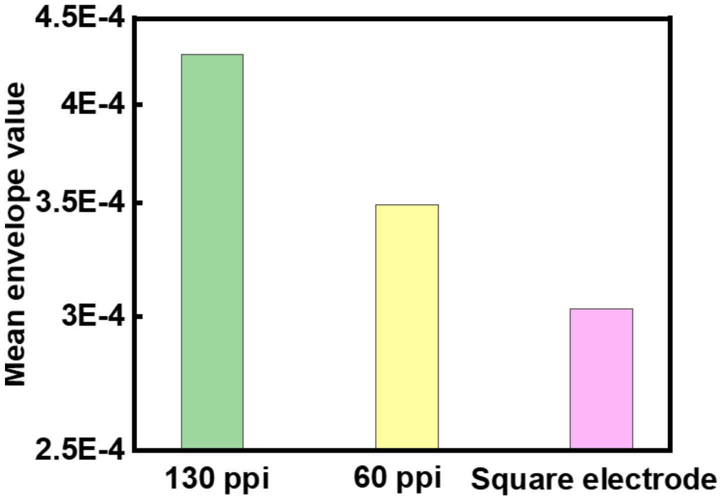

Supplementary Figure 20. Mean envelope value obtained from FFT analysis of the impedance fluctuations of 130 ppi, 60 ppi, and a highly ordered square electrode.

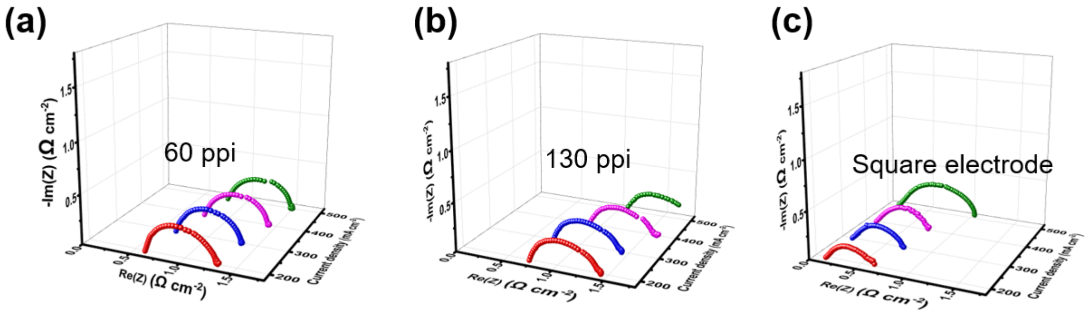

Supplementary Figure 21. Electrochemical impedance spectroscopy measurements of the electrolyzer equipped with (a) 60 ppi, (b) 130 ppi nickel foam, and (c) 3D-printed grid electrodes under current densities varying from 200 mA cm^{-2} to 500 mA cm^{-2}.

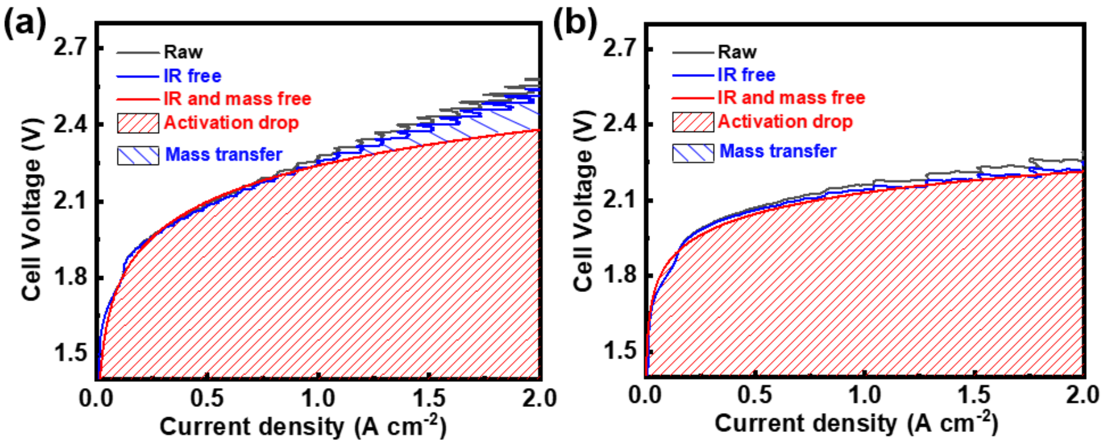

Supplementary Figure 22. Breakdown of ohmic, mass transport, and activation losses for (a) 60 ppi nickel foam-based polarization curve and (b) highly-ordered square electrodes-based polarization curve.

Supplementary Table 1 Reported alkaline water electrolyzer (AWE) performances with different porous substrates, electrode architectures, and operating conditions.

Substrate	Anode	Cathode	Performance	Temp.	Electrolyte	Separator	Ref
Perf-Ni	VPS-NiAl	VPS-NiAlMo	~1.91 V @1 A/cm^2	80°C	30 wt% KOH	Zirfon 500	2
Ni-Foam	LDH-NiFe	Raney Ni	~2 V @1 A/cm^2	80°C	30 wt% KOH	Zirfon 500	3
Ni-Foam	LDH-NiFe	Raney Ni	1.83 V @1 A/cm^2	80°C	30 wt% KOH	300 µm ZrO_2-based separator	3
Ni-Foam	Ni-Foam	Raney Ni	1.74 V @0.3 A/cm^2	80°C	32.5 wt% KOH	Zirfon 500	4
Steel mesh	α-Nickel hydroxide	Co-sputtered Ni and Mo	1.84 V @0.3 A/cm^2	70°C	30 wt% KOH	Zirfon Pearl, unknown thickness	5
Ni-Foam	DC sputtered Ni	DC sputtered Ni	~2.24 V @0.9 A/cm^2	80°C	25 wt% KOH	Zirfon 500	6
Ni-Foam	RF sputtered Ni	RF sputtered Ni	~2.29 V @0.9 A/cm^2	80°C	25 wt% KOH	Zirfon 500	6
Perf-Ni	Porous Ni-based electrode	Mo incorporated porous Ni	1.84 V @1 A/cm^2	70°C	30 wt% KOH	Zirfon 500	7
Square electrode	NiFe-LDH	Pt	2.13 V @2 A /cm^2 (10 A/cm^3)	Ambient temperature	30 wt% KOH	Zirfon	This work

Reference

1. K. Dastafkan, Q. Meyer, X. Chen and C. Zhao, *Small*, 2020, **16**, 2002412.
2. M. Schalenbach, G. Tjarks, M. Carmo, W. Lueke, M. Mueller and D. Stolten, *J. Electrochem. Soc.*, 2016, **163**, F3197.
3. H. I. Lee, M. Mehdi, S. K. Kim, H. S. Cho, M. J. Kim, W. C. Cho, Y. W. Rhee and C. H. Kim, *J. Membr. Sci.*, 2020, **616**, 118541.
4. C. Karacan, F. P. Lohmann-Richters, M. Shviro, G. P. Keeley, M. Müller, M. Carmo and D. Stolten, *J. Electrochem. Soc.*, 2022, **169**, 054502.
5. B. Zayat, D. Mitra and S. Narayanan, *J. Electrochem. Soc.*, 2020, **167**, 114513.
6. W.-B. Han, I.-S. Kim, M. Kim, W. C. Cho, S.-K. Kim, J. H. Joo, Y.-W. Lee, Y. Cho, H.-S. Cho and C.-H. Kim, *Electrochim. Acta.*, 2021, **386**, 138458.
7. F. Egert, D. Ullmer, S. Marx, E. Taghizadeh, T. Morawietz, M. Gerle, T. A. Le, L. P. Campo Schneider, I. S. Biswas and R. E. Wirz, *Adv. Energy Mater.*, 2025, **15**, 2405285.